Development of a self-consistent free-form approach for studying the three-dimensional morphology of a thin film

Igor V. Kozhevnikov
Institute of Crystallography, Leninsky Prospect 59, Moscow 119333, Russia

Luca Peverini* and Eric Ziegler†
European Synchrotron Radiation Facility, BP 220, 38043, Grenoble Cedex, France

(Received 21 June 2010; revised manuscript received 12 September 2011; published 28 March 2012)

A method capable of extracting the depth distribution of the dielectric constant of a thin film deposited on a substrate and the three power spectral density (PSD) functions characterizing its roughness is presented. It is based on the concurrent analysis of x-ray reflectivity and scattering measurements obtained at different glancing angle values of the probe beam so that the effect of roughness is taken into account during reconstruction of the dielectric constant profile. Likewise, the latter is taken into account when determining the PSD functions describing the film roughness. This approach is using a numerical computation iterative procedure that demonstrated a rapid convergence for the overall set of data leading to a precise description of the three-dimensional morphology of a film. In the case of a tungsten thin film deposited by dc-magnetron sputtering onto a silicon substrate and characterized under vacuum, the analysis of the x-ray data showed the tungsten density to vary with depth from 95% of the bulk density at the top of the film to about 80% near the substrate, where the presence of an interlayer, estimated to be 0.7 nm thick, was evidenced. The latter may be due to diffusion and/or implantation of tungsten atoms into the silicon substrate. In the reconstruction of the depth profile, the resolution (minimum feature size correctly reconstructed) was estimated to be of the order of 0.4–0.5 nm. The depth distribution of the dielectric constant was shown to affect the roughness conformity coefficient extracted from the measured x-ray scattering distributions, while the deposition process increased the film roughness at high spatial frequency as compared to the virgin substrate. On the contrary, the roughness showed a weak influence on the dielectric constant depth profile extracted, as the sample used in our particular experiment was extremely smooth.

DOI: 10.1103/PhysRevB.85.125439 PACS number(s): 61.05.C−, 81.15.Aa, 68.55.J−, 68.35.Ct

I. INTRODUCTION

X-ray reflectivity and scattering methods are unique tools for studying the morphology of thin films.[1,2] They are able to provide a quantitative analysis of the roughness evolution of a film under various treatments and to infer the depth distribution of the dielectric constant within the film in a nondestructing way. However, up to now, these two topics have been investigated independently of each other on the base of simplified assumptions. In the analysis of the film roughness, it is typically assumed that the film density is constant over depth and the substrate roughness unaffected by the film coating deposited above it, as done, e.g., in our recent *in situ* and real-time studies of the growth and erosion of tungsten films.[3–5] Evidently a number of materials and process conditions do not fulfill such ideal situation. Likewise, during the reconstruction of the dielectric constant profile from x-ray reflectivity measurements, the effect of interfacial roughness is usually neglected or described in a simplified manner. The introduction of a Nevot-Croce factor to account for the contribution of each interface roughness to the amplitude reflectance is a common example of such a practice.

As the depth profile of the dielectric constant, extracted from reflectivity measurements, affects the wave field inside the film and, hence, modifies the scattering pattern, questions arise regarding the modification of the dielectric constant profile when roughness is taken into consideration. Conversely, it would be important to assess the influence of the depth distribution profile of the dielectric constant on the film roughness parameters. This paper is precisely devoted to the development of a method for extracting information on the film morphology simultaneously in depth (dielectric constant profile) and in the lateral direction (roughness). Although this approach seems to be the most sensible one, the practical realization remains to be demonstrated. The tungsten film represents an ideal case study because a large amount of information on this system was acquired earlier through several *in situ* experiments regarding growth and erosion. The description obtained after analysis of the x-ray reflectivity and scattering data collected using straightforward procedures described in Refs. 3–5 will allow us to make a comprehensive evaluation of the self-consistent method presented here.

II. RECONSTRUCTION OF THE DIELECTRIC CONSTANT DEPTH DISTRIBUTION WITHIN THE FILM

The reconstruction on the base of angular reflectivity measurements $R(\theta)$ of the depth profile of the dielectric constant $\varepsilon(z)$ of a thin film coated on a substrate is a well-known inverse problem. The standard approach consists in modeling the $\varepsilon(z)$-distribution with a function of several unknown parameters found by least-square fitting to the experimental data. Evidently, this approach requires a sophisticated understanding of the sample internal structure. When unable to conceive an adequate model to describe an unknown structure, a model-independent approach to solve the inverse problem is highly desired.

At present, several free-form approaches to reconstruct the dielectric constant profiles from x-ray or neutron

reflectivity data have been developed. Among very general approaches one should mention the maximum entropy method, the Bayesian spectral analysis,[6] and the parameterization of $\varepsilon(z)$-distribution using cubic B splines or sine/cosine basis.[7] However, these methods may result in ambiguous and unphysical solutions due to insufficient information.[6,7] Causes include the limited incoming photon flux, the noise of the detector that limits the range of grazing angles θ over which useful data can be measured and the fact that present detectors can only measure intensities $R(\theta) = |r(\theta)|^2$ [modulus of the amplitude reflectance $r(\theta)$]. Therefore, as indicated in Refs. 6 and 7, any additional knowledge about the sample is of the highest importance. Even a good estimation of the overall sample thickness or information on whether the polarizability is higher on the top or on the bottom of a sample, can contribute to a correct reconstruction of the dielectric constant profile.

Bengu *et al.*[8] have developed an approach to find a set of feasible, physically grounded solutions. The approach is based on the genetic algorithm used together with the phase inversion to impose a set of general constraints that will limit the number of possible solutions. Similarly, the approach developed in Ref. 9 and used in the present paper selects, among an infinite number of possible solutions, those providing the desired (modeled) amplitude reflectivity behavior at large $q \equiv k \sin\theta$ (where k $=2\pi/\lambda$), the wave vector component normal to the surface.

The modeling of the amplitude reflectivity $r(q)$ at large q is possible in the frame of a general model of reflecting media. A distribution $\varepsilon(z)$ is declared as having a point of discontinuity of the nth order if $\varepsilon(z)$ and its n-1 derivatives $\varepsilon'(z), \ldots, \varepsilon^{(n-1)}(z)$ are continuous functions at the point z, while its nth derivative $\varepsilon^{(n)}(z)$ suffers a steplike variation at this point, i.e., $\Delta^{(n)}(z) \equiv \varepsilon^{(n)}(z-0) - \varepsilon^{(n)}(z+0) \neq 0$. Notice that, in the case of a point of discontinuity of zeroth order, the dielectric constant itself undergoes a steplike variation. Following the approach developed in Ref. 9, we state that the dielectric constant profile can be reconstructed uniquely, or, at least, that there exists a finite number of possible solutions to the inverse problem, if the number and the order of the points of discontinuity of the dielectric function and the distances between them are known. The dominating term of the asymptotic series describing the amplitude reflectance at the large grazing angle, i.e., at large q, writes as follows:

$$r(q) \cong -k^2 \left(\frac{i}{2q}\right)^{n+2} \sum_{j=1}^{m} \Delta^{(n)}(z_j) \exp(2iqz_j), \qquad (1)$$

where the summation is over all the points of discontinuity. The z axis is supposed to point into the direction of the depth of the substrate. Hence, the reflectivity at large q behaves as

$$R(q) = |r(q)|^2 \cong \frac{k^4}{(2q)^{2n+4}} \left\{ \sum_j [\Delta^{(n)}(z_j)]^2 + 2 \sum_{l>j} \Delta^{(n)}(z_j)\Delta^{(n)}(z_l) \cos(2qh_{jl}) \right\}, \qquad (2)$$

where $h_{jl} = z_l - z_j$ is the distance between the lth and jth points of discontinuity. The absorption and refraction of radiation in matter are neglected when the total thickness of a layered structure is small enough: $L \ll \lambda \sin\theta/|1-\varepsilon|$.

As seen, the reflectivity behaves in average as $R(q) \sim 1/q^{2n+4}$ at large q and oscillates around the average curve if there is more than one point of discontinuity. Hence, by analyzing the rapidity of decrease of the reflectivity and the period of the oscillations, we can establish the order and the number of points of discontinuity as well as the distances between them.

Considering now the case in which points of discontinuity are only of the *zero*th order, we can introduce the following function:

$$F(x) = \frac{16}{k^4(q_{\max} - q_{\min})} \int_{q_{\min}}^{q_{\max}} [q^4 R(q) - G] \cos(2qx)\, dq$$
$$G = \frac{1}{q_{\max} - q_{\min}} \int_{q_{\min}}^{q_{\max}} q^4 R(q)\, dq \qquad (3)$$

where the integration is performed over the measurable range of the parameter $q = k \sin\theta$. The function $F(x)$ in Eq. (3) is similar to the traditional autocorrelation function of the dielectric constant profile derivative used in the analysis of the x-rays reflectivity data, while differing by two specific features discussed in Appendix A. The function $F(x)$ oscillates near the zero value and has many maxima or minima, the position of the extrema depending, in general, on the values of $q_{\max}$ and $q_{\min}$. At the same time, there is a set of stable extrema placed at the fixed points $x = h_{ji}$ independently of $q_{\max}$ and $q_{\min}$. Assuming the angle $\theta_{\min}$ to be greater than the critical angle of total external reflection, the value of $F(x)$ at these points is found to equal to

$$F(h_{ji}) = \Delta(z_j)\Delta(z_i) + (\text{nonresonant terms}), \qquad (4)$$

where the nonresonant terms are typically small and decrease as $1/(q_{\max} - q_{\min})$ with increasing $q_{\max}$ values. Hence, by analyzing the function $F(x)$ at various $q_{\max}$ and $q_{\min}$, we can find the distances between all the points of discontinuity present in the $\varepsilon(z)$-distribution. In addition, all double products $\Delta(z_j)\Delta(z_i)$ can be found as well. Then, based on Eqs. (2) and (3), we can find the following sum:

$$\sum_j [\Delta(z_j)]^2 = \frac{2}{q_{\max} - q_{\min}} \int_{q_{\min}}^{q_{\max}} \left[\frac{8q^4}{k^4} R(q) - \sum_{h_{ji}} F(h_{ji}) \cos(2qh_{ji}) \right] dq. \qquad (5)$$

Considering Eqs. (4) and (5) as a system of equations in unknowns, $\Delta(z_j)$, we can estimate the variation of the dielectric constant at every interface. Note that the system has typically four possible solutions, $\Delta(z_j)$, the correct one being identified on the basis of additional physical considerations. A more detailed discussion of the problem of uniqueness is given in Appendix A. From the analysis of the measurable part of the reflectivity curve, we can formulate a general model for the $\varepsilon(z)$-distribution, describing the main features observed in the reflectivity curve.

For direct reconstruction of the dielectric constant profile, we apply a special numerical procedure detailed in Ref. 9. In addition, the absorption of radiation in matter is neglected

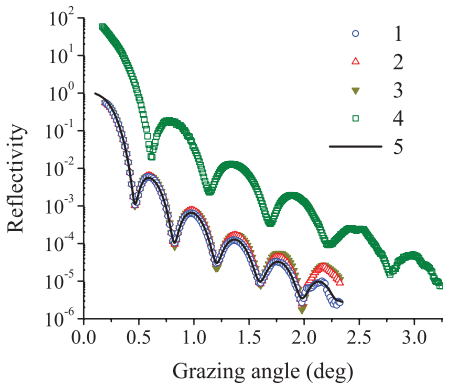

FIG. 1. (Color online) Reflectivity measured at a fixed x-ray energy of 17.5 keV and variable grazing angle from two tungsten films, 5.1 nm (1) and 3.6 nm (4) thick, deposited onto identical superpolished silicon substrates (curve 4 is shifted vertically for clarity). Curves 2 and 3 are the refined specular reflectivity of the thicker film. The solid curve 5 is the result of calculation accounting for the dielectric constant profile shown in Fig. 6 and the PSD functions shown in Fig. 5.

when reconstructing the $\varepsilon(z)$-distribution. In practice, the level of ambiguity is greater than expected, as we need to determine two functions $\Re[\varepsilon(z)]$ and $\Im[\varepsilon(z)]$, *a priori* unknown. In our case of a tungsten film measured at an x-ray energy of 17.5 keV, absorption can be neglected outside the total external reflection region when the film thickness does not exceed 6 to 7 nm.[9] For films composed of lighter materials, this upper limit in thickness is greater. Neglecting absorption means that when processing, we should exclude experimental data where the effect of absorption on the reflectivity is large, i.e., data close to the critical angle of total external reflection. Evidently, some information about the sample studied will be lost, including the dielectric constant of the substrate that defines the critical angle. However, the loss of this information is not crucial, because (a) the substrate also influences the rest of the reflectivity curve so that its dielectric constant can still be determined and (b) the dielectric constant of the substrate is known *a priori*.

In Fig. 1, curves 1 and 4 present the reflectivity measured as a function of the grazing angle for two tungsten films of different thickness deposited by magnetron sputtering onto superpolished Si substrates. After deposition and during x-ray measurements, the samples were kept under vacuum. A detailed description of the experimental setup used for deposition and subsequent reflectivity and scattering measurements is given elsewhere (Refs. 3–5).

First, we verify that the reflectivity at large θ values decreases slightly faster than a $1/q^4$ law. Nevertheless, bearing in mind that the presence of roughness results in a decrease of the reflectivity, we can assume that the ε(z)-distribution will contain, at least, one point of discontinuity of zeroth order. Second, as there are well-pronounced oscillations in the reflectivity curves, we can assume that there is more than one point of discontinuity. The function *F(x)* calculated in slightly different intervals of q values (grazing angles ranging from $\theta_{\min} = 0.5{-}0.6^\circ$ to $\theta_{\max} = 2.0{-}2.3^\circ$) is presented in Fig. 2(a) for the thicker film. As seen, the function *F(x)* has only one extremum, indicated by an arrow, that has a

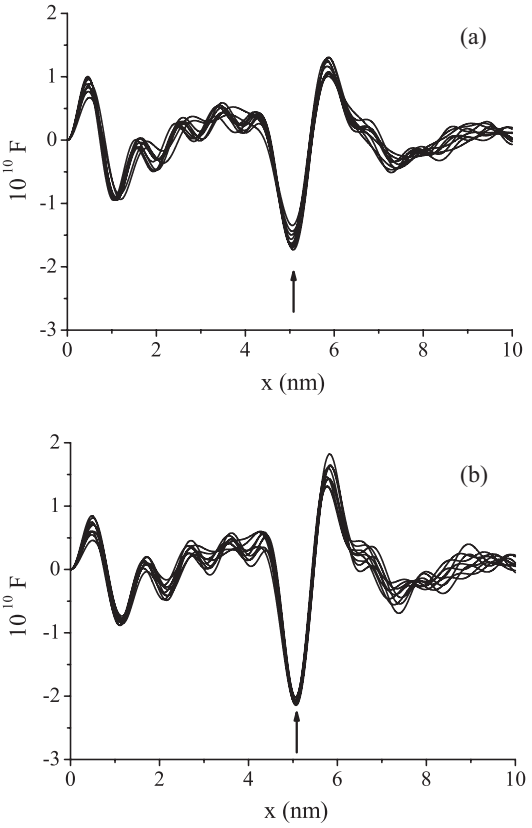

FIG. 2. Illustration of the film thickness determination with the use of Eq. (3) for the thicker film studied. The analysis is based on the measured reflectivity [graph (a)] and on the refined specular reflectivity [graph (b)]. The film thickness proved to be equal to $h = 5.07 \pm 0.03$ nm (a) or $h = 5.06 \pm 0.01$ nm (b).

stable position independently of the values of $q_{\max}$ and $q_{\min}$. Hence, there are two points of discontinuity, the distance between them being $h = 5.07 \pm 0.03$ nm. For the thinner tungsten film, the thickness is found to be $h = 3.63 \pm 0.03$ nm. The negative value of the function $F(x)$ at the extremum point indicates that the steplike variations of the dielectric constant at the discontinuity points are of opposite signs. Clearly, these points find their origin in the presence of vacuum-film and film-substrate interfaces. Notice that the value $F(x)$ at the extremum point is not constant and changes slightly when varying the integration interval $[q_{\min}, q_{\max}]$. We attribute this effect to roughness because the reflectivity decrease is not entirely consistent with a $1/q^4$ law as assumed when deriving Eq. (4). Following Eqs. (4) and (5), in the case of the 5.1-nm-thick film, the values of the function $F(x)$ in its extremum and of the average reflectivity curve are given by the product $\Delta(0)\Delta(h) = -(1.5 \pm 0.2).10^{-10}$ and by the sum $\Delta^2(0) + \Delta^2(h) = (4.1 \pm 0.4).10^{-10}$, respectively.

The accurate reconstruction of the dielectric constant profile $\varepsilon(z)$ was done numerically using a computer procedure described in details in Ref. 9. The routine uses a merit function with a specific form to guarantee the asymptotic behavior of the amplitude reflectance [Eq. (1)] outside the angular interval, where experimental data is available, as well as the best possible agreement, within experimental errors, between measured and calculated reflectivity curves inside this interval.

Besides the fact that $\varepsilon(z) = 1$ for $z < z_1$ and $\varepsilon(z) = \varepsilon_+ =$ const for $z > z_{m+1}$, let us suppose that the function $\varepsilon(z)$ has m points of zero-order discontinuity $z_1, \ldots, z_m$. Let us now divide each interval $[z_j, z_{j+1}](j = 1, \ldots, m)$ into l sublayers of equal thickness $d_j = (z_{j+1} - z_j)/l$, where l is a parameter of the procedure, and assume the dielectric permeability to be constant inside each sublayer. Then the ε(z)-distribution is a function of $N = lm$ values of ε inside each sublayer, the ε-value in the depth of the substrate and the number of sublayers inside each interval.

Let us introduce the following merit function $\mathrm{MF_R}$ (case of points of zeroth-order discontinuity):

$$\mathrm{MF}_R(\varepsilon_1, \ldots, \varepsilon_{N+1}, N) = \sum_{j=1}^{M} [\log R(\theta_j) - \log R_{\exp}(\theta_j)]^2 + Q \sum_{\substack{i=1,\ldots,N \\ i \neq i_1, i_2, \ldots i_m}} (\varepsilon_{i+1} - \varepsilon_i)^2, \qquad (6)$$

where $R_{\exp}(\theta_j)$ and $R(\theta_j)$ are the measured and calculated reflectivity values at the grazing angle θ_j, M the number of experimental data points, and Q a parameter of the numerical procedure. The summation is over all boundaries between the sublayers excluding the points of discontinuity $i_1, i_2, \ldots, i_m$, where the function ε(z) changes abruptly. The role of the second term in the merit function is to ensure a smooth ε(z)-distribution, and more importantly, the asymptotic behavior of the reflectivity [Eq. (2)] (see Ref. 9 for a detailed discussion and the generalization of the merit function [Eq. (6)] for points of discontinuity of arbitrary orders). Then, the numerical computation problem consists of finding the sequence $\varepsilon_1, \varepsilon_2, \ldots, \varepsilon_{N+1}$ that minimizes the merit function $\mathrm{MF_R}$. A high enough value of the parameter Q should be used to provide the necessary asymptotic of the reflectivity at large q, while the difference between calculated and measured reflectivity curves should lie within the experimental errors. Notice that a similar stabilizing function was used in Ref. 7 to bias the solution toward the most physically reasonable one.

In the presence of two points of discontinuity (our example), one can anticipate from Eqs. (1) and (2) that four different asymptotic dependencies $r(q)$ may lead to the same asymptotic behavior of the reflectivity, $R(q)$, i.e., the inverse problem has four possible solutions. Unlike Eq. (1), Eq. (2) is invariant when substituting $\Delta(0)$ and $\Delta(h)$ for one another, or when substituting simultaneously $\Delta(0)$ by $-\Delta(0)$ and $\Delta(h)$ by $-\Delta(h)$, meaning the asymptotic behavior permits neither to differentiate whether a given steplike variation Δ of the function $\varepsilon(z)$ occurs at the points $z = 0$ or $z = h$, nor to determine the sign of the dielectric constant variation at the points of discontinuity.

However, additional information can help select the right solution. First, because the dielectric constant of a material at x-ray wavelength is less than unity, the two solutions out of four resulting in a negative variation of the dielectric function ($\Delta(0) < 0$) at the vacuum-film interface can be discarded. There are different ways of choosing the solution between the two remainders. As the amplitude reflectance, contrary to the reflectivity, depends on the values of $\Delta(0)$ and $\Delta(h)$ separately, we can uniquely find the solution corresponding to reality by measuring the phase of the reflected wave. A method for extracting this phase directly from *in situ* reflectivity measurements of a growing film is discussed in recent works.[10]

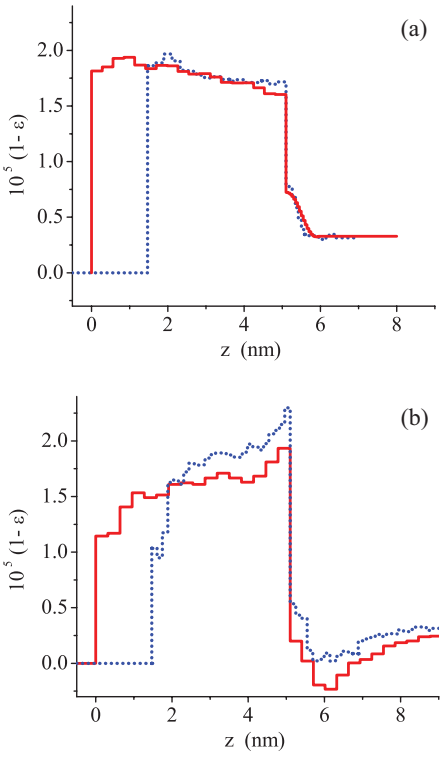

FIG. 3. (Color online) Reconstructed dielectric constant profiles for two tungsten films deposited on silicon substrates. The film thickness is equal to 5.1 nm (solid curve) or 3.6 nm (dotted curve). Figures 3(a) and 3(b) correspond to two possible solutions to the inverse problem of x-ray reflectometry providing a positive value of $\Delta(0)$. The roughness effect was not taken into account. The z axis is pointing toward the depth of the substrate.

A simpler, though more intuitive, approach for selecting the adequate $\varepsilon(z)$-distribution among a limited number of possible solutions consists of analyzing the dielectric constant profiles of samples presenting slightly different parameters. In our case it is sufficient to compare the dielectric constant profiles of two films of different thickness. An example is presented in Figs. 3(a) and 3(b), where two, out of four, possible depth distributions of the dielectric constant, providing a negative polarizability of tungsten ($\varepsilon_f < 1$), are shown. In all cases the starting guess for minimizing the merit function was a tungsten film of uniform density deposited on a Si substrate. By varying the film density in the starting guess, we obtained four (and only four) different solutions to the inverse problem. The curves are very similar to each other in Fig. 3(a) and quite different in Fig. 3(b). Moreover, the dielectric constant of the thicker film in Fig. 3(b) exceeds unity at the depth $z \sim 6$ nm, which is unphysical at the working wavelength. Therefore, we conclude that only Fig. 3(a) corresponds to reality. Notice, in addition, that the product $\Delta(0)\Delta(h) = -1.58.10^{-10}$ and the sum $\Delta^2(0) + \Delta^2(h) = 4.07 \cdot 10^{-10}$ found for the $\varepsilon(z)$-distribution correspond to the values obtained above from the analysis of the function $F(x)$. Figure 3(a) manifests two characteristic features of the dielectric function distribution. First, the tungsten density increases appreciably from about

80% of the tungsten bulk density at the beginning of deposition up to 95% near the top of the film. At present a decrease of the tungsten density near the substrate surface is not totally understandable. One possible explanation for this decrease could be the lack of surface cleaning of the Si substrate prior to W film deposition. It is, indeed, well-known that any surface exposed to air is covered with an adhesion layer, typically 1 to 2 nm thick, consisting mainly of molecules of hydrocarbons, water, and oxygen sticking to the surface. Therefore, we can expect that, at the initial stage of W film growth, a chemical interaction of the tungsten atoms with the molecules of such an adhesion layer may result in the formation of tungsten oxides and/or carbides, thus resulting in a decrease of the film density near the substrate surface. To justify this hypothesis, a comparative study of the growth of a tungsten film on cleaned (e.g., by ion etching) and uncleaned Si surfaces would be necessary. Second, a well-pronounced diffusion layer is seen near the surface of the substrate, which we would attribute to the implantation and/or diffusion of tungsten atoms into silicon during deposition. The description of the fine structure of the interlayer observed in these samples is obviously limited by the depth resolution of the method, estimated to 0.5 nm. The details on this problem of crucial importance to the reconstruction of the dielectric function are discussed in Appendix B. So, we conclude that the x-ray reflectivity curves measured from tungsten films deposited onto silicon substrates are described adequately in the frame of a model assuming the dielectric function to undergo a steplike variation at the film-vacuum and film-substrate interfaces. Hence, the depth distribution of the dielectric constant can be written in the following form:

$$\varepsilon_0(z) = 1 + [\varepsilon_f(z) - 1]\, H(z) + [\varepsilon_s(z) - \varepsilon_f(z)]\, H(z-h), \tag{7}$$

where h is the film thickness and $H(z)$ is the steplike Heaviside function so that $H(z<0)=0$ and $H(z>0)=1$, whereas $\varepsilon_f(z)$ and $\varepsilon_s(z)$ are continuous functions of z. In the simplest case of a uniform film, $\varepsilon_f(z)$ and $\varepsilon_s(z)$ are constants.

III. DETERMINATION OF THE PSD FUNCTIONS CHARACTERIZING THIN-FILM ROUGHNESS

In the previous section we analyzed the x-ray reflectance of a layered sample neglecting the effect of roughness, i.e., assuming the dielectric constant [Eq. (7)] to be only a function of the depth $\varepsilon(\vec{r}) = \varepsilon_0(z)$. In this case the surface corresponding to a cut through the sample along a plane $z =$ constant is a surface of constant dielectric function ε. However, as no real sample can be perfectly smooth at the scale of short wavelength x-ray radiation, we need to describe the spatial distribution of the dielectric constant as $\varepsilon(\vec{r}) = \varepsilon_0(z - \zeta(\vec{\rho},z))$, where the two-dimensional vector $\vec{\rho}$ lies in the XY-plane and the stochastic function ζ describes inhomogeneities of different types so that a surface of constant ε is described by the equation $z - \zeta(\vec{\rho},z) =$ const. Such a representation of the dielectric constant implies that diffuse scattered x-ray radiation is caused by surface or interface roughness and by volume inhomogeneities. In the frame of the perturbation theory on the function ζ, the dielectric constant perturbation responsible for off-plane x-ray scattering and decrease in specular reflectance is represented as two first terms of a Taylor series:

$$\Delta\varepsilon(\vec{r}) \equiv \varepsilon(\vec{r}) - \varepsilon_0(z) \approx -\zeta(\vec{\rho},z)\varepsilon_0'(z) + \frac{\zeta^2(\vec{\rho},z)}{2}\varepsilon_0''(z).$$

This expression indicates that it is the region of the sample in which the dielectric constant varies quickly that mainly conditions the intensity of the scattered radiation. Evidently, in our case (see Fig. 3), the vacuum-film and film-substrate interfaces, the location of the abrupt changes, constitute the main contributions to scattering. Therefore, we will neglect below the contribution of the volume scattering as compared to the one from interfacial roughness. Then the spatial distribution of the dielectric constant can be written as an evident generalization of Eq. (7)

$$\begin{aligned}\varepsilon(\vec{r}) = 1 &+ [\varepsilon_f(z) - 1]H(z - \zeta_f(\vec{\rho})) \\ &+ [\varepsilon_s(z) - \varepsilon_f(z)]H(z - h - \zeta_s(\vec{\rho})),\end{aligned} \tag{8}$$

where the stochastic functions $\zeta_s(\vec{\rho})$ and $\zeta_f(\vec{\rho})$ describe the topographic relief of the substrate and of the film, respectively.

In general, the angular distribution of the scattered radiation intensity (differential scattering cross-section) is a function of two angles: the scattering angle θ between the direction of observation (detector) and the sample surface and the azimuthal scattering angle. In our experiments the horizontal beam size is set to a large value (5 mm) to favor a high intensity at the detector. Moreover, because the scattering pattern in the azimuthal (horizontal) direction is very narrow, we integrate the intensity in this direction. In the frame of the film model depicted in Eq. (8) and in the first-order perturbation theory approximation, the scattering cross-section integrated in the azimuthal direction from a rough isotropic film reads

$$\begin{aligned}\Pi(\theta,\theta_0) &= \frac{1}{W_{\text{inc}}}\frac{dW_{\text{scat}}}{d\theta} \\ &= \frac{k^3}{16\pi\sin\theta_0}\{|\Delta(0)\,\psi_0(0,\theta_0)\psi_0(0,\theta)|^2 \text{PSD}_{\text{ff}}(p) \\ &\quad + |\Delta(h)\,\psi_0(h,\theta_0)\psi_0(h,\theta)|^2\,\text{PSD}_{\text{ss}}(p) \\ &\quad + 2\Re[\Delta(0)\Delta^*(h)\,\psi_0(0,\theta_0)\psi_0(0,\theta)\psi_0^*(h,\theta_0) \\ &\quad \times \psi_0^*(h,\theta)]\text{PSD}_{\text{sf}}(p)\}; \\ p &= \frac{1}{\lambda}\,|\cos\theta - \cos\theta_0|\end{aligned} \tag{9}$$

where $\Delta(0) = 1 - \varepsilon_f(0)$ and $\Delta(h) = \varepsilon_f(h) - \varepsilon_s(h)$ are the variations of the dielectric constant at the vacuum-film and film-substrate interfaces, respectively, and θ_0 is the grazing angle of the probe beam. The function $\psi_0(z,\theta)$ describes a plane wave falling from the vacuum region onto a film whose surface is perfectly smooth, and the dielectric constant depth distribution is nonuniform. $\psi_0(z,\theta)$ has the following asymptotic form:

$$\psi_0(z,\theta) \sim \begin{cases} \exp(ikz\sin\theta) + r(\theta)\exp(-ikz\sin\theta), & \text{at } z \to -\infty \\ t(\theta)\exp(i\kappa(\theta)z), & \text{at } z \to +\infty \end{cases},$$

where $\kappa(\theta) = k\sqrt{\varepsilon_+ - \cos^2\theta}$ is the Z-projection of the wave vector in the depth of the substrate with the dielectric constant $\varepsilon_+ = \varepsilon_0(z \to +\infty)$.

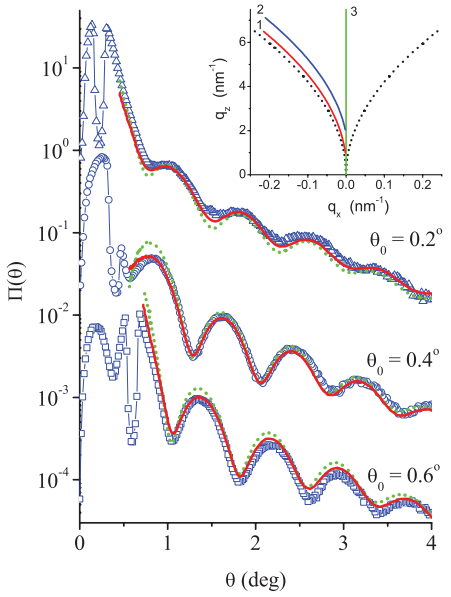

FIG. 4. (Color online) Normalized scattering intensity (symbols) versus scattering angle of a 5.1-nm-thick tungsten film measured at three grazing angles θ_0 (0.2°, 0.4°, and 0.6°) at an x-ray energy of 17.5 keV. The lines represent the scattering distributions calculated using either the simple model of a film with constant density (dotted curves) or taking into account the dielectric constant profile extracted from reflectivity measurement (solid curves). For clarity the curves corresponding to different θ_0 are shifted vertically by a factor of 10. The sharp minimum at the angle $\theta = \theta_0$ corresponding to the specular reflected beam is due to the presence of a beam stop to avoid the saturation of the detector. *Inset:* Detector scans in reciprocal space for $\theta_0 = 0.2°$ (1) and 0.6° (2). Straight line 3 indicates the specular reflectivity scan and dotted curves show the boundaries of inaccessible q space.

In the simplest case of a uniform film, the field amplitudes ψ_0 at the film interfaces can be expressed in an explicit analytical form, while for an arbitrary depth-graded dielectric function, they must be obtained numerically as a solution of a one-dimensional wave equation. The polarization effects have been neglected because the grazing incidence angle is small. The one-dimensional power spectral density (PSD) functions[11] are determined as

$$\mathrm{PSD}_{ij}(p) = 2\int \langle \zeta_i(\vec{\rho})\zeta_j(0)\rangle \cos(2\pi p\rho)\, d\rho\,, \quad \text{with} \quad i,j = \{s,f\}\,, \tag{10}$$

where the angular brackets denote an ensemble averaging and p is the spatial frequency. The functions $\mathrm{PSD}_{ss}(p)$ and $\mathrm{PSD}_{ff}(p)$ describe the roughness of the substrate and of the external film surface, respectively, and $\mathrm{PSD}_{sf}(p)$ determines the statistical correlation (conformity) between film and substrate roughness.

The general formulae, the applicability of the perturbation theory in the x-ray region and its interrelation with the distorted-wave Born approximation,[12] are discussed elsewhere.[13,14]

The experimental scattering distributions of the 5.1-nm-thick tungsten film measured at three different grazing angles of the probe beam θ_0 are presented in Fig. 4 (symbols). The insert in the figure shows the detector scan in the reciprocal space $q_z = k(\sin\theta + \sin\theta_0)$, $q_x = k(\cos\theta - \cos\theta_0)$. Note that the q_x values spanning from $(-2.2\cdot 10^{-3})$ to (-0.22) nm^{-1} were used when processing the data. Then, we use Eq. (9) to form a system of linear algebraic equations dependent on the three PSD functions mentioned above. In principle, for each value of the spatial frequency p, the unknown PSD functions can be found without any modeling. However, it is a well-known fact that the solution of a system of algebraic equations is often an ill-conditioned problem, meaning that a small experimental error in the measured scattering distributions may result in a large error in the PSD functions. In our case, the direct solving of the system effectively resulted in strongly oscillating PSD functions and, moreover, in nonphysical negative values of PSD_{ss} and PSD_{ff} in some intervals of the spatial frequency, thus suggesting to use the regularization procedure[15] described below. The three unknown functions $\mathrm{PSD}_{ij}(p)$ are found from minimization of the following merit function

$$\mathrm{MF}_{\mathrm{PSD}} = \sum_i \int_{p_{\min}}^{p_{\max}} \left[\frac{\Pi^{\exp}\left(p,\theta_0^{(i)}\right) - \Pi^{\mathrm{cal}}\left(p,\theta_0^{(i)}\right)}{\Pi^{\exp}\left(p,\theta_0^{(i)}\right)}\right]^2 dp + Q \sum_{i,j=s,f} \int_{p_{\min}}^{p_{\max}} \left[\frac{d\ln(\mathrm{PSD}_{ij}(p))}{d\ln p}\right]^2 dp, \tag{11}$$

where $\Pi^{\exp}$ and Π^{cal} denote the differential scattering cross-sections measured and calculated at different grazing angles $\theta_0^{(i)}$ of the probe beam. The second term in Eq. (11) is nothing but a stabilizing operator introduced to provide the necessary smoothness of the solution $\mathrm{PSD}_{ij}(p)$ in which the parameter Q should be large to obtain a smooth solution to the problem, while keeping the difference between calculated and measured scattering cross-sections within the experimental error. Usually, these two conflicting conditions result in a unique choice of the Q value. The values of the PSD functions at 100 different spatial frequency values lying in the interval $[3.5\cdot 10^{-4}, 3.5\cdot 10^{-2}$ nm$^{-1}]$ were considered as fitting parameters so that the PSD functions were derived directly from the measured scattering cross-sections without using any model. When minimizing $\mathrm{MF}_{\mathrm{PSD}}$, the only constraint placed for finding the solution was on the conformity coefficient characterizing the vertical correlation between film and substrate roughness that should not exceed unity:

$$K(p) = \frac{\mathrm{PSD}_{sf}(p)}{\sqrt{\mathrm{PSD}_{ss}(p)\cdot \mathrm{PSD}_{ff}(p)}} \leqslant 1. \tag{12}$$

To guarantee this inequality, we introduced a new unknown function $f(p)$ within $\mathrm{PSD}_{sf}(p)$ so that $\mathrm{PSD}_{sf}(p) = \sqrt{\mathrm{PSD}_{ff}(p)\cdot \mathrm{PSD}_{ss}(p)}\cdot \exp[-f^2(p)]$. The starting guess for all PSD functions was the PSD_0 function of the virgin substrate measured before film deposition and shown in Fig. 5. Within the measurable range of spatial frequency, PSD_0 is well described by an inverse power law $1/p^{1+2\alpha}$ with a Hurst exponent $\alpha \approx 0.14$. At first, after Refs. 3–5, we made the *a priori* assumption that PSD_{ss} was unaltered by the film deposition. In addition, we used the simplest model possible, i.e., a uniform film, with a constant density of 17 g/cm^3. This value provides the best fitting accuracy on the reflectivity curve

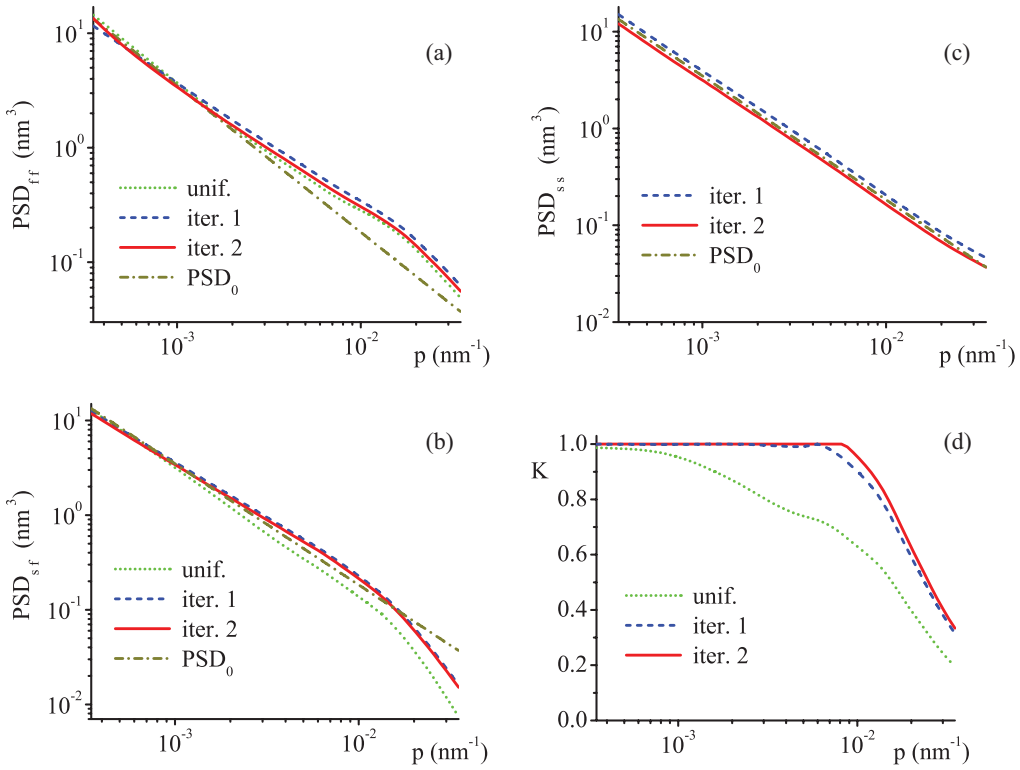

FIG. 5. (Color online) Functions PSD_{ff} (a), PSD_{sf} (b), and PSD_{ss} (c) of the 5.1-nm-thick tungsten film extracted directly from the measured scattering distributions. PSD_0 is the function corresponding to the virgin Si substrate averaged over statistical oscillations. The dotted green curves show the PSD functions deduced using the simple model of a uniform film, i.e., of constant density, and assuming the substrate roughness to be unchanged after film deposition. The dashed blue and solid red curves correspond to the results obtained at different steps of the iteration procedure. (d) Roughness conformity coefficient [Eq. (12)] obtained at different steps of the iterative procedure.

measured as a function of the deposition time at fixed grazing angle ($\theta_0 = 0.4°$). The resulting PSD functions, PSD_{ff} and PSD_{sf}, are shown in Figs. 5(a) and 5(b) [dotted green (gray) curves]. The fitting accuracy on the scattering distributions is presented in Fig. 4 [dotted green (gray) curves]. The hump observed on the PSD_{ff} function shown in Fig. 5(a) [dotted green (gray) curve] as compared to the PSD_0 curve, confirms the development of intrinsic roughness in the high spatial frequency domain. Nevertheless, the root-mean-square (rms) roughness over the measurable range of spatial frequency presented increases only slightly, from 0.11 nm for the initial substrate to 0.13 nm after deposition of a 5.1-nm-thick tungsten film. Previous *in situ* studies on tungsten (Refs. 3–5) also evidenced a very slow increase of roughness during film growth. At large spatial frequency the PSD_{ff} function of the external film surface behaves like an inverse power law $1/p^{1+2\alpha}$ with a Hurst exponent α estimated to 0.22 ± 0.04. This value correlates with the one ($\alpha = 0.18 \pm 0.02$) obtained in Ref. 4. In addition, the rapid decrease of the function PSD_{sf} at a large spatial frequency substantiates the exponential decrease [Fig. 5(d), dotted green (gray) curve] of the roughness conformity coefficient with the spatial frequency and demonstrates an absence of conformity of the small-scale roughness, in agreement with Refs. 3–5.

Notice the poor fitting accuracy of the dotted curve in Fig. 4 with a difference between the measured and calculated scattering cross-sections up to 40–50%. Decreasing the parameter Q in the merit function MF_{PSD} did not improve significantly the situation, while promoting the appearance of nonphysical oscillations in the PSD functions. A slightly better fitting accuracy could be obtained when considering PSD_{ss} (substrate) as an unknown in the minimization procedure. However, that resulted in a function $PSD_{ss}(p)$ with an intensity three to four times lower than the function $PSD_0(p)$ of the virgin substrate, meaning the smoothing of the roughness over the whole range of measurable spatial frequency. Such a smoothing effect is unrealistic from a physical point of view.

Let us now consider as unknown the three PSD functions describing a rough film deposited on a substrate, while taking into account the depth distribution of the dielectric constant derived above. We use the same minimization procedure of the merit function [Eq. (11)] and the values of the three PSD functions at 100 different spatial frequency values as fitting parameters. Equation (9) for the scattering cross-section is still valid, while the field amplitudes at the film interfaces are found numerically using the $\varepsilon(z)$-distribution shown in Fig. 6, iteration 1. The resulting PSD functions, shown in Fig. 5, (iteration 1) are similar in shape to those found with the model of uniform film, while their absolute values are different. As a result, the roughness conformity coefficient [Fig. 5(d)] manifests a substantial increase of conformity at high spatial frequency compared to the uniform film model. The PSD function of the substrate after film deposition (PSD_{ss}) was found to be close to that of the virgin substrate (PSD_0).

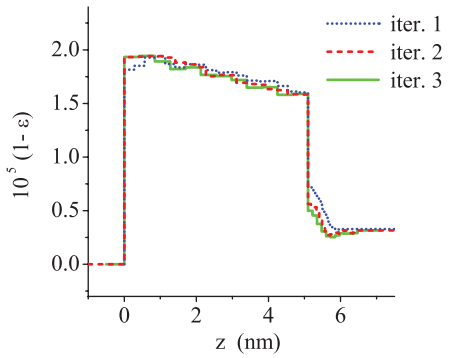

FIG. 6. (Color online) Comparison of the dielectric constant depth profiles found at different steps of the iteration procedure.

The difference between the functions PSD_{ss} and PSD_{sf} found with the models of uniform and depth-graded films can be appreciated by examining Eq. (9) describing the scattering cross-section. Indeed, the electrodynamics multiplier factors in front of the PSD functions depend on the dielectric constant variation at the film-substrate interface. As the variation of the dielectric constant at the interface between the depth-graded film and the substrate is lower than in the case of the uniform film (by a factor of 1.5–2), the function PSD_{ss} and PSD_{sf} should be increased to be able to describe the mean value and the amplitude of the oscillations observed in the scattering patterns. The accuracy of the solution corresponding to the depth-graded film is shown in Fig. 4 (red solid curves). This time, the difference between the measured and the calculated scattering cross-sections does not exceed 15%, which is comparable with the measurement errors, while the root-mean-squared deviation between the curves is less than 5%, which is far better than for the uniform film model.

IV. ITERATIVE PROCEDURE

In the previous sections we reconstructed the depth distribution of the dielectric constant, neglecting the effect of roughness, and then deduced all three PSD functions of a rough film, taking into account this $\varepsilon(z)$-distribution (iteration 1). Now we will continue the iteration procedure shown schematically in Fig. 7. In the second iteration we envisaged, first, to reconstruct the depth distribution of the dielectric constant taking roughness into account, and then, to refine once more the PSD functions. Thereafter, we compared the results of two iterations [the found $\varepsilon(z)$-distributions and the PSD functions]. If the difference between results is small enough, the iterative procedure is finished; otherwise, the dielectric constant profile and the PSD functions are refined again until the desired convergence (difference in the results of two subsequent iterations) is achieved.

The procedure of the dielectric constant profile refinement is rather complex. First of all, we indicate the expression for the specular reflectivity R of a rough depth-graded film derived in the frame of the perturbation theory, while conserving all terms in σ^2 and using the model Eq. (8) to describe the three-dimensional (3D) distribution of the dielectric function

$$R = R_0 - 2\Re[r_0^*(\Delta r_1 + \Delta r_2)] \tag{13}$$

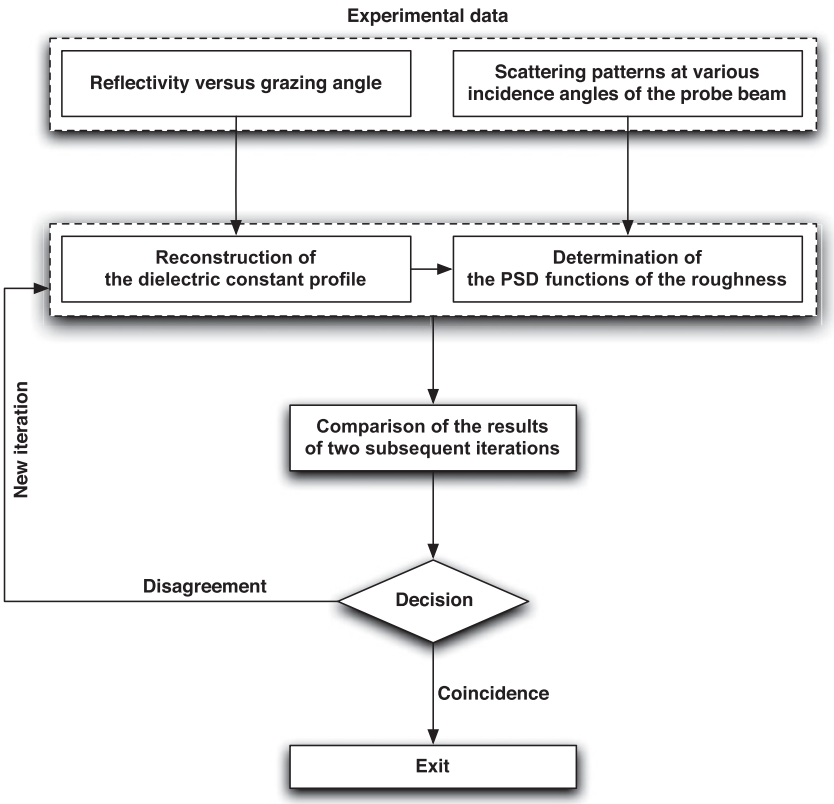

FIG. 7. Flowchart describing the iterative procedure.

$$\Delta r_1 = -\frac{ik}{2\sin\theta_0}\left[\sigma_f^2\Delta(0)\,\psi_0(0,\theta_0)\frac{d\psi_0}{dz}(0,\theta_0) + \sigma_s^2\Delta(h)\,\psi_0(h,\theta_0)\frac{d\psi_0}{dz}(h,\theta_0)\right] \tag{14}$$

$$\Delta r_2 = \frac{ik^4}{8\pi\sin\theta_0}\left\{\Delta^2(0)\,\psi_0^2(0,\theta_0)\int \mathrm{PSD}_{\mathrm{ff}}(p)\frac{\psi_0(0,\theta)\,\psi_1(0,\theta)}{W(\theta)}\sin\theta\,d\theta + \Delta^2(h)\,\psi_0^2(h,\theta_0)\int \mathrm{PSD}_{\mathrm{ss}}(p)\frac{\psi_0(h,\theta)\,\psi_1(h,\theta)}{W(\theta)}\sin\theta\,d\theta\right.$$
$$\left. + 2\Delta(0)\Delta(h)\,\psi_0(0,\theta_0)\psi_0(h,\theta_0)\int \mathrm{PSD}_{\mathrm{sf}}(p)\frac{\psi_0(h,\theta)\,\psi_1(0,\theta)}{W(\theta)}\sin\theta\,d\theta\right\} \tag{15}$$

where $R_0 = |r_0|^2$ is the reflectivity of a perfectly smooth depth-graded film and σ_s and σ_f are the rms roughness of the substrate and of the film. The function $\psi_1(z,\theta)$ describes a plane wave arriving in the film from the substrate side and having the following asymptotic form:

$$\psi_1(z,\theta) \sim \begin{cases} \tilde{t}(\theta)\exp(-ikz\sin\theta), & \text{at } z \to -\infty \\ \exp(-i\kappa(\theta)z)) + \tilde{r}(\theta)\exp(i\kappa(\theta)z), & \text{at } z \to +\infty \end{cases}$$

$W(\theta) = \psi_0'\psi_1 - \psi_0\psi_1' = 2it(\theta)\kappa(\theta) = 2i\tilde{t}(\theta)k\sin\theta$ is the Wronskian. The other functions and parameters were described previously.

The main problem is that the reflectivity calculation requires the knowledge of the PSD functions over the entire spatial frequency range, i.e., for p values from zero to infinity, while they were only measured in a finite interval. Hence, we need to extrapolate the PSD functions outside this interval using arguments as physically reasonable as possible. In the high spatial frequency region, we will consider that the functions $\mathrm{PSD}_{\mathrm{ss}}$ and $\mathrm{PSD}_{\mathrm{ff}}$ follow a fractal-like law $\sim 1/p^{1+2\alpha}$ and the function $\mathrm{PSD}_{\mathrm{sf}}$ an exponential law. At low spatial frequency, all PSD functions practically coincide with each other and ensure total conformity at large-scale roughness. For extrapolation of the PSD functions in the low spatial frequency range, we use the following simplest model for the PSD function of the substrate used widely in optics[16]

$$\mathrm{PSD}_{\mathrm{ss}}(p) = \frac{2}{\sqrt{\pi}}\frac{\Gamma(\alpha+1/2)}{\Gamma(\alpha)}\frac{\sigma^2 a}{(1+a^2p^2)^{\alpha+1/2}}, \tag{16}$$

where σ is the rms roughness in the $[0,\infty[$ spatial frequency interval, a is the correlation length, $\alpha \approx 0.14$ the exponent found, while the numerical coefficient containing gamma functions is chosen to warrant the normalization condition $\int_0^\infty \mathrm{PSD}(p)\,dp = \sigma^2$. If the correlation length is large enough $a \gg 1/p_{\min}$, where $p_{\min}$ is the minimal spatial frequency measured in the experiment, Eq. (16) tends to the asymptotical form $\mathrm{PSD}_{\mathrm{ss}}(p) \sim \sigma^2/(a^{2\alpha}p^{1+2\alpha})$, demonstrating that the ratio σ/a^α can only be found that way and that the values of σ and a cannot be obtained separately. This situation corresponds to the conditions of our experiment with $p_{\min} = 1\cdot 10^{-3}$ nm^{-1}, and Fig. 5 only attests that the correlation length is greater than 10 μm. Hence, the rms roughness cannot be found uniquely. At the same time, the reflectivity [Eq. (13)] depends heavily on the value of σ and, hence, on the extrapolation of the PSD function in the low spatial frequency range. To overcome this problem in our experiments, we measured the total reflectivity coefficient instead of the specular reflectivity

$$R_\Sigma(\theta_0) = R(\theta_0) + \mathrm{TIS}(\theta_0);$$
$$\mathrm{TIS}(\theta_0) = \int \Pi(\theta,\theta_0)\,d\theta, \tag{17}$$

where TIS is the total integrated scattering. The total reflectivity characterizes the total intensity of radiation that is redirected back to vacuum after interaction with the rough film, i.e., the specularly reflected part and the part scattered by roughness. In contrast to specular reflectivity, TIS is independent of the PSD function extrapolation at low frequency. This feature will greatly simplify the implementation of the self-consistent method. Notice that, for a sufficiently large value of the longitudinal correlation length of roughness, the width of the scattering pattern is much smaller than the typical angular width of a reflectivity variation and roughness of different interfaces are totally conformal. In this case the specular reflectance and the total integrated scattering are described by the well-known Debye-Waller factor

$$R \cong R_0[1-(2k\sigma\sin\theta_0)^2]; \quad \mathrm{TIS} \cong R_0\,(2k\sigma\sin\theta_0)^2$$

so that the total reflectivity [Eq. (17)] is very close to the reflectivity R_0 of a perfectly smooth sample.

In fact, if we extrapolate all three PSD functions describing the sample in the range of the low spatial frequency values, via Eq. (16), over which an exponent $\alpha \approx 0.14$ was found above, and if we calculate the total reflectivity R_Σ [Eq. (17)] via Eqs. (9) and (13)–(15) for various correlation lengths a ranging from 10 μm to 1 mm, the R_Σ values differ only by the third significant digit, while the value of σ^2 increases by a factor of 3.6. So, in accordance with Eqs. (13) and (17) and independently of the type of PSD function extrapolation used in the low spatial frequency range, we can determine the specular reflectivity R_0 of the depth-graded sample (which would be equivalent to the case of perfectly smooth interfaces)

$$R_0 \cong R_\Sigma + 2\Re[r_0^*(\Delta r_1 + \Delta r_2)] - \mathrm{TIS}, \tag{18}$$

where R_Σ is the quantity measured in our experiment, and TIS, $\Delta r_{1,2}$, and r_0 in the right side of Eq. (18) are values calculated from the PSD functions and the $\varepsilon(z)$-distribution obtained previously. The refined specular reflectivity [Eq. (18)] for the 5.1-nm-thick tungsten film is shown in Fig. 1 (curve 3). The difference between the measured total reflectivity (curve 1) and the specular reflectivity expected from a perfectly smooth film is only noticeable at large grazing angles, demonstrating once more that the total reflectivity is close to the reflectivity of a perfectly smooth sample. The difference between curves 1 and 2 in Fig. 1 is only conditioned by the effect of small-scale roughness, whose rms height is very small.

Now, based on the reflectivity curve corrected for the roughness effect, we can refine the depth distribution of the dielectric constant using the procedure described in Sec. III. First of all, we find that the reflectivity curve 2 in Fig. 1, in contrast to the measured one, is well consistent with a $1/q^4$ law at large grazing angles. Therefore, the extremum of the function $F(x)$ is much more stable [see Fig. 2(b)] regarding both its position in the x direction and its value $F(h)$. The refined distance between points of discontinuities is practically the same as found above $h = 5.06 \pm 0.01$ nm and the error on the determination of h is decreased by a factor of three. The dielectric constant variations at the film interfaces can be obtained via Eqs. (4) and (5) within an accuracy of about 6%: $\Delta(0) = (1.93 \pm 0.12).10^{-5}$ and $\Delta(h) = -(1.06 \pm 0.06) \cdot 10^{-5}$. The refined depth distribution of the dielectric function presented in Fig. 6, iteration 2 is very close to that found during the first iteration, i.e., when roughness was not taken into account. However, it is more uniform near the top of the film and the diffusion layer inside the substrate is less pronounced. It is also consistent with the results obtained in Ref. 10 for thicker tungsten films (up to 25 nm), where the thickness of the diffusion layer inside the Si substrate and of the near substrate layer having a decreased tungsten density was estimated to be of about 1 nm and 2.5–3 nm, respectively. The dielectric constant variations at the interfaces deduced from Fig. 6, iteration 2, $\Delta(0) = 1.93 \cdot 10^{-5}$ and $\Delta(h) = -1.03 \cdot 10^{-5}$, coincide with those obtained during the preliminary analysis of the function $F(x)$. Then, we refined the PSD functions. However, no significant changes are observed on Fig. 5, iteration 2 when compared to iteration 1. The fitting accuracy of the scattering cross-sections and of the conformity coefficient [Fig. 5(d)] are also nearly the same. It is interesting to observe in Fig. 5(a) that the $\mathrm{PSD_{ff}}$-function for iteration 2 resembles the one obtained with the model of uniform film and with the assumption of the substrate roughness to remain unchanged during deposition. This fact justifies the validity of our earlier results (Refs. 3–5). On the contrary, the roughness conformity coefficient depends significantly on the film model, stressing the importance of taking properly the dielectric constant profile into account when performing a quantitative analysis of the vertical correlation of roughness.

The third iteration performed as detailed above shows very little differences with the PSD functions deduced after the first and second iterations, thus leading to marginal corrections on the reflectivity. As a result, the refined reflectivity curves 2 and 3 in Fig. 1 are almost indistinguishable, and the dielectric constant depth distribution essentially unchanged (see Fig. 6, iteration 3). The PSD functions are equivalent to those found at the second iteration and are not plotted in Fig. 5. This example demonstrates the rapid convergence of the iterative procedure, at least in the case of smooth samples. Two iterations were sufficient to derive the three PSD functions describing a rough film and to reconstruct the depth distribution of its dielectric constant. For the scattering cross-sections, the accuracy of the description is illustrated in Fig. 4 by the comparison of the experimental (symbols) and the solid curves. For the reflectivity, it is illustrated by the comparison in Fig. 1 of the measured total reflectivity R_Σ (curve 1), with the solid curve 5 calculated using the PSD functions presented in Fig. 5 and the reconstructed ε(z)-distribution shown in Fig. 6. In summary, the iterative procedure presented could certainly be improved, which could be valuable for studying samples presenting a larger rms roughness. The method of reconstruction of the dielectric constant described above is based on the specular reflectivity. Although its quantity can be estimated by subtracting the embedded diffuse scattering component, this procedure is not well defined because it requires extrapolation of the measured part of the scattering pattern into the range of the scattering angles close to the angle of specular reflection. The problem has been demonstrated above with extrapolation of the PSD functions into the range of low spatial frequencies. Therefore, the specular reflectivity is deduced from the measurement of the total reflectivity corrected for the roughness effect. A more logical iterative procedure could be developed by introducing in Eq. (6) the total reflectivity instead of the specular one, the former being calculated using the PSD functions and Eqs. (9) and (13)–(15). However, the computing time necessary to minimize the merit function Eq. (6) is expected to be much longer.

V. CONCLUSION

In the study of the 3D morphology of a film deposited on a substrate, a method has been developed to determine simultaneously the depth distribution of its dielectric constant and the three PSD functions characterizing its roughness. The approach is based on the simultaneous analysis of the reflectivity curve and of a set of scattering cross-sections measured at different grazing angles of the x-ray probe beam. A numerical computation iterative procedure has been developed to take into account the roughness effect during the reconstruction of the dielectric constant profile and vice versa, the depth distribution of the dielectric constant during the determination of the PSD functions of the film roughness. The iterative procedure was demonstrated to converge quickly to describe precisely the whole set of experimental data.

The main results of the study are now summarized. We demonstrated that the depth distribution of the dielectric constant affects significantly the roughness conformity coefficient extracted from the measured scattering cross-sections. Conversely, the roughness influences the profile of the dielectric constant extracted from the measured reflectivity curve, although in our case of very smooth samples, this effect is rather weak. The density of a tungsten film deposited by magnetron sputtering onto a silicon substrate is not constant and varies with depth from about 80% of the bulk density near the substrate up to 95% at the top of the film. During deposition an interlayer, about 0.7 nm thick, appears at the top of the substrate. It may be due to diffusion and/or implantation of tungsten atoms into the silicon substrate. The deposition of a tungsten film results in an increase of high spatial frequency roughness.

We note that the study of the three-dimensional morphology of a layered structure will increase in complexity with the number of layers in the sample for two major reasons. First, above a certain thickness, absorption cannot be neglected anymore and, hence, two *a priori* unknown functions $\Re[\varepsilon(z)]$ and $\Im[\varepsilon(z)]$ should be reconstructed from the measured reflectivity curve. In this case the problem of ambiguity gets more pronounced. This issue is not analyzed in the present

paper. Second, the number of *a priori* unknown PSD functions of the roughness of a layered structure increases dramatically as $n(n+1)/2$ with the increasing number of interfaces n. (We have in this case n autocorrelation functions of the roughness of different interfaces and $n(n-1)/2$ cross-correlation ones.) Evidently, it is impossible to deduce all these functions from the experimental scattering distributions directly, i.e., without using a model to describe the roughness variation with depth. This is the real limitation of applicability of our free-form approach in the study of multilayer structures. At the same time, we believe that the only physically justified way to develop an adequate model of roughness development and interlayer formation during multilayer structure growth is to study, at first, simpler structures with a small number of layers (2 to 3 or, may be, 4), where our free-form approach seems to be quite practicable.

ACKNOWLEDGMENT

I.V.K. acknowledges the support of the ISTC (Grant project No. 3124).

APPENDIX A

Our approach for the reconstruction of the dielectric constant profile is based essentially on the preliminary Fourier-analysis of the reflectivity curve via Eq. (3). The function $F(x)$ introduced there differs by two special features from the traditional autocorrelation function of the dielectric constant profile derivative used in the analysis of the x-ray reflectivity data (see, e.g., Ref. 6). First, we normalize $F(x)$ in such a way that the resonance summand in Eq. (4) is independent of the integration interval. Such normalization results in stable extrema and (a) distinguishes clearly the peaks determined by the distances between discontinuity points from a variety of collateral ones and (b) determines the pair products $\Delta_i \Delta_j$ of the dielectric constant variations at the discontinuity points. In our opinion, this last feature, not discussed in the literature, may be of extreme importance for identifying the correct model to describe the sample under study. Second, we introduced the summand G in the integrand in Eq. (3) to increase the sensitivity of the approach and allow stable peaks of very low magnitude to be displayed. The importance of this summand will be illustrated in the following example.

Let us analyze the x-ray reflectivity ($E = 17.5$ keV) of a 2-nm-thick Si film deposited onto the bulk Si substrate, the density of the film being only 5% less than the bulk density. Assuming the reflectivity to be measured up to a maximum grazing angle $\theta_{\max} = 2.5^\circ$ [Fig. 8(a)] and calculating the function $F(x)$ in the traditional form found in the literature with $G = 0$ at slightly different $q_{\max}$ and $q_{\min}$values, we obtain curves that present a well-pronounced maximum at $x = 0$ [Fig. 8(b)] with a value equal to $F(0) = \sum_j [\Delta(z_j)]^2$. However, the large amplitude collateral oscillations of this peak at $x > 0$ hide an expected stable extremum at $x = 2$ nm, and thus, we cannot distinguish the presence of the film. At the same time, if we use the function $F(x)$ in the form Eq. (3) containing the summand $G \neq 0$, the large peak disappears, and the stable maximum at $x = 2$ nm is now clearly observed [Fig. 8(c)]. Therefore, the function F in the form Eq. (3) is able to detect even a small variation of the dielectric constant at the interfaces (the points of discontinuity).

The problem of uniqueness in the dielectric constant profile reconstruction is of extreme importance. First of all, we note that the number of possible solutions (four) is independent of the number of discontinuity points when all distances between points h_{ij} and all pair products $\Delta_i \Delta_j$ are different. Let us consider three subsequent discontinuity points z_{j-1}, $z_j = z_{j-1} + h_{j-1,j}$, $z_{j+1} = z_j + h_{j,j+1}$ and the corresponding sequence of dielectric constant variations in these points: Δ_{j-1}, Δ_j, Δ_{j+1}. One of the extrema of the function $F(x)$ matches the distance $h_{j-1,j+1} = h_{j-1,j} + h_{j,j+1}$ between the $(j-1)$th and $(j+1)$th points. As we supposed that all h_{ij} are different, the only possibility to change the sequence of discontinuity points, while keeping the same value of $h_{j-1,j+1}$ (position of extremum), consists of reversing the order of intervals between the neighboring points, i.e., to change the initial sequence of the three discontinuity points in the following way: z_{j-1}, $z_j = z_{j-1} + h_{j,j+1}$, $z_{j+1} = z_j + h_{j-1,j}$. Simultaneously, we should reverse the sequence of the dielectric constant variations Δ_{j+1}, Δ_j, Δ_{j-1} to maintain the values of the extrema $\Delta_{j-1}\Delta_j$ and $\Delta_j\Delta_{j+1}$ corresponding to the distances between neighboring points $h_{j-1,j}$ and $h_{j,j+1}$. As this consideration should be valid for any j, we conclude that among the variety of different permutations, only one, namely, the mirror representation of the initial sequence of discontinuity points and of the dielectric constant variations

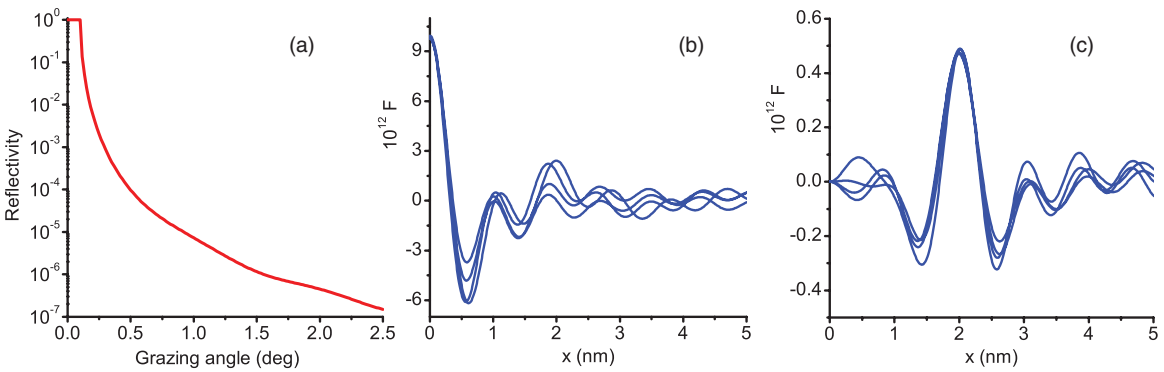

FIG. 8. (Color online) (a) Reflectivity versus grazing angle (at $E = 17.5$ keV) of a 2-nm-thick Si film on the bulk Si substrate, the film density being 0.95 of the bulk one. (b) and (c) Determination of the film thickness with the use of a conventional autocorrelation function of the dielectric constant profile derivative (b) and via Eq. (3) (c).

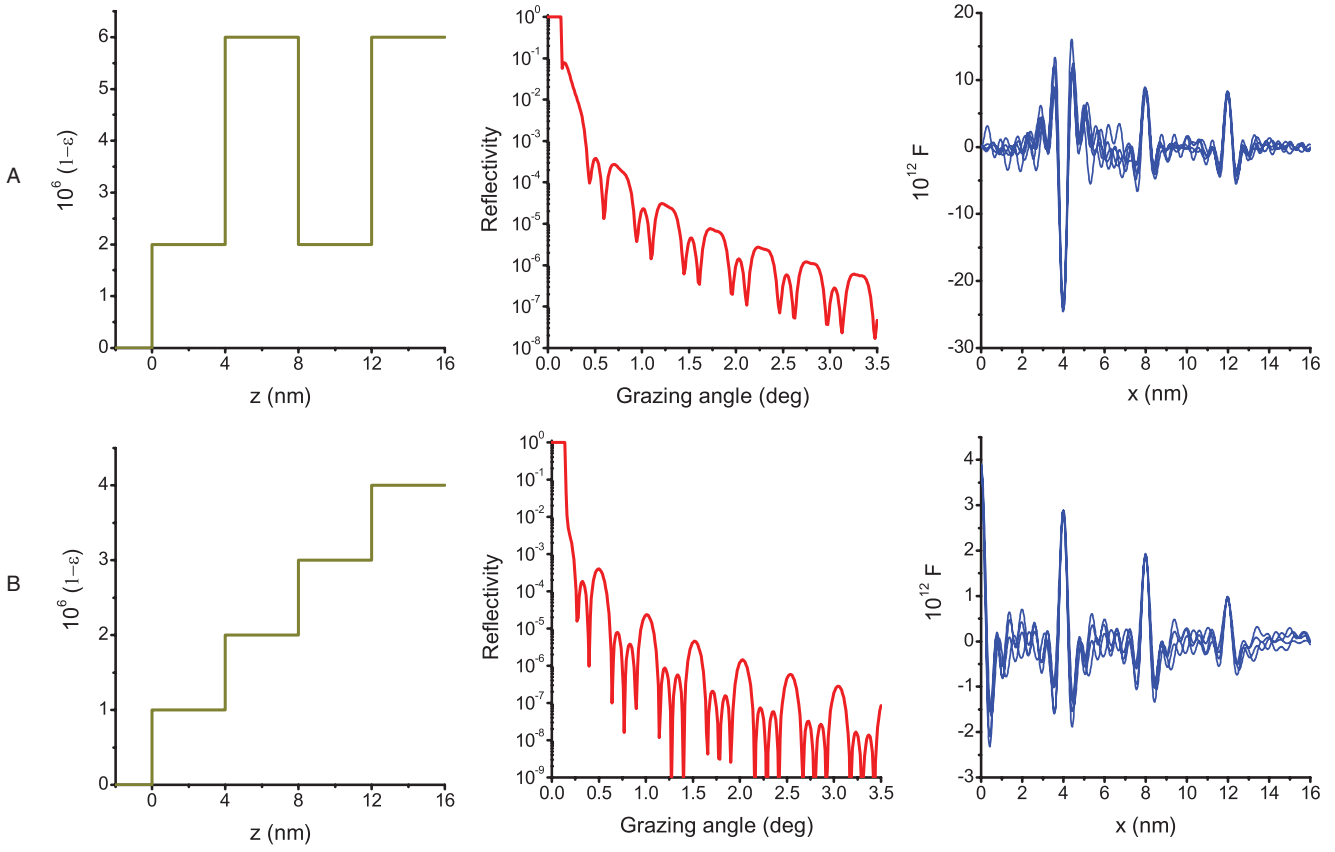

FIG. 9. (Color online) Two model examples (rows A and B) of three-layer samples with identical thickness for each layer ($h = 4$ nm). The dielectric constant profiles are shown in the left column, the reflectivity (at E = 17.5 keV) in the middle column, and the functions $F(x)$ in the right column.

results in the same extrema of the function $F(x)$. Hence, there are only two different sequences of discontinuity points ensuring the same asymptotic behavior of the reflectivity at large grazing angles:

$$\{\Delta_1(z=0),\ \Delta_2(z=h_{12}),\ldots,\ \Delta_{n-1}(z=h_{12}+\cdots + h_{n-2,n-1}),\ \Delta_n(z=h_{12}+\cdots+h_{n-1,n})\}$$
$$\{\Delta_n(z=0),\ \Delta_{n-1}(z=h_{n-1,n}),\ldots,\ \Delta_2(z=h_{n-1,n}+\cdots + h_{23}),\ \Delta_1(z=h_{n-1,n}+\cdots+h_{12})\}. \quad \text{(A1)}$$

Two additional solutions of the inverse problem follow immediately from Eq. (A1) by replacement of Δ_j by $-\Delta_j$.

As already pointed out in Ref. 6, the case of several layers (distances between points of discontinuity) of equal thickness is more difficult to analyze. To help clarify this point, let us consider below a three-layer model with films of constant density while neglecting absorption. While the function $F(x)$ for films of different thicknesses would have six extrema, the case of films of identical thickness h leads to a function $F(x)$ with three extrema placed in the points $x = h$, $x = 2h$, and $x = 3h$. The value of the function in these points is equal to

$$F(h) = \Delta_1\Delta_2 + \Delta_2\Delta_3 + \Delta_3\Delta_4, \quad F(2h) = \Delta_1\Delta_3 + \Delta_2\Delta_4,$$
$$F(3h) = \Delta_1\Delta_4. \quad \text{(A2)}$$

In absence of *a priori* information about the sample, such a function $F(x)$ would suggest a simple two-layer sample model with film thicknesses h and $2h$. Is it possible to determine the correct number of layers composing the sample based on the sole reflectivity curve and without performing additional experiments? Surprisingly, it is indeed possible because, in parallel to the distances between the points of discontinuity, we have additional information about the sample, namely, the pair products $\Delta_i\Delta_j$ of the dielectric constant variation in these points determined by the peak values of the function $F(x)$. As an illustration of our approach, let us consider two examples.

The first example of a three-layer sample with equal film thickness is presented in Fig. 9, row A. If we assume the simplest two-layer model, i.e., only three points of discontinuity, and denote the dielectric constant variation in these points as $\tilde{\Delta}_1$, $\tilde{\Delta}_2$, and $\tilde{\Delta}_3$, we obtain three equations: $\tilde{\Delta}_1\tilde{\Delta}_2 \approx -24$, $\tilde{\Delta}_1\tilde{\Delta}_3 \approx 8$, and $\tilde{\Delta}_2\tilde{\Delta}_3 \approx 8$. By multiplying them, we obtain an unphysical result $(\tilde{\Delta}_1\tilde{\Delta}_2\tilde{\Delta}_3)^2 < 0$, thus clearly demonstrating the incorrectness of a two-layer model. Similarly, in the general case of n discontinuity points ($n-1$ layers) and different distances h_{ij} between them, we can calculate the product of all peak values $P = \prod F(h_{ij})$. One can check that each Δ_j occurs in this product $n-1$ times so that $P = (\Delta_1\Delta_2\cdots\Delta_n)^{n-1}$. Therefore, the sign of the product P, always positive in the case of an odd number of discontinuity points, can be used as a signature for the correctness of the model.

A second example of three-layer sample is shown in Fig. 9, row B. Here, for illustrative purpose, we used a conventional function $F(x)$ by setting $G = 0$. The peak

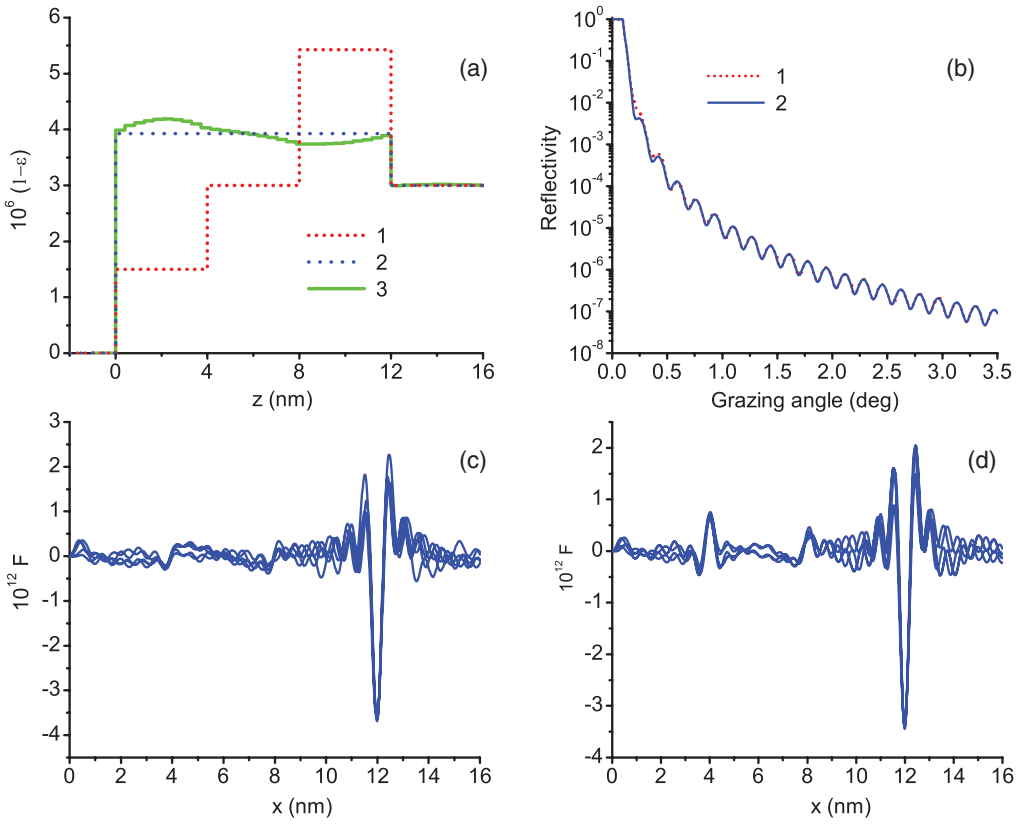

FIG. 10. (Color online) (a) Dielectric constant profiles of three-layer (1) and one-layer (2) samples presenting the same reflectivity at large grazing angles. Curve 3 is the refined profile of the one-layer sample model found as a solution of the inverse problem and provides the same reflectivity as a three-layer sample at any grazing angle. (b) Reflectivity versus grazing angle (at E = 17.5 keV) of three-layer (1) and one-layer (2) samples. (c) Function F(x) of the three-layer sample. (d) Same as in Fig. 10(c) assuming the density of the uppermost and the lowermost film to be changed by $+5\%$ and -5%, respectively.

at $x = 0$ influences slightly the neighboring peak in this example. As seen, all products $\tilde{\Delta}_i\tilde{\Delta}_j$ are positive, i.e. $(\tilde{\Delta}_1\tilde{\Delta}_2\tilde{\Delta}_3)^2 > 0$, and the dielectric constant variations in the three discontinuity points (assuming the two-layer model) can be easily found: $\tilde{\Delta}_1^2 \approx 1.5$, $\tilde{\Delta}_2^2 \approx 6.0$, $\tilde{\Delta}_3^2 \approx 0.7$. Then, we obtain $\tilde{\Delta}_1^2 + \tilde{\Delta}_2^2 + \tilde{\Delta}_3^2 \approx 8.2$, a value twice the peak value observed at $x = 0$, which stresses again the inadequacy of a two-layer model to describe the "experimental" data.

In the general case of n points of discontinuity with different thicknesses h_{ij}, we can evaluate $n(n-1)/2$ products $\Delta_i\Delta_j$ and the value of $\Delta_1^2 + \cdots + \Delta_n^2$, i.e., we have $n(n-1)/2 + 1$ equations for n unknowns Δ_i. For $n > 2$, the number of equations exceeds the number of unknowns, and the equations agree with each other only in the frame of a model with the correct number of films except in very specific cases, which, probably, never occur in practice, although of possible fundamental interest.

A specific case similar to the one discussed in Ref. 6 is presented in Fig. 10(a), profile 1. In this three-layer model with films of equal thickness, the dielectric constant variations in the discontinuity points Δ_i are chosen to provide simultaneously

$$\Delta_1\Delta_2 + \Delta_2\Delta_3 + \Delta_3\Delta_4 = 0 \quad \text{and} \quad \Delta_1\Delta_3 + \Delta_2\Delta_4 = 0. \tag{A3}$$

Then, in accordance with Eq. (A2), we observe the only peak of the function $F(x)$, while a small stable feature at $x \approx 3.7$ nm still persists [Fig. 10(c)]. We can conclude that the situation is similar to that of the reflection from a single film, i.e., with the case of two points of discontinuities, the distance between them being 12 nm. Denoting the dielectric constant variations in these points as $\tilde{\Delta}_1$ and $\tilde{\Delta}_2$ and solving the system of equations $\tilde{\Delta}_1\tilde{\Delta}_2 = \Delta_1\Delta_4$ and $\tilde{\Delta}_1^2 + \tilde{\Delta}_2^2 = \Delta_1^2 + \cdots + \Delta_4^2$, we can design a single-layer structure [Fig. 10(a), profile 2], whose reflectivity at large grazing angles coincides with that of the three-layer structure, apart from small differences observable at $\theta \sim 0.2^\circ - 0.45^\circ$ [Fig. 10(b)]. As $n = 2$, the number of equations is exactly equal to the number of unknowns $\tilde{\Delta}_{1,2}$ and the equations always have a solution. Therefore, in very specific cases, when the dielectric constants of the films exactly match Eq. (A3), we are truly incapable of determining the number of discontinuity points.

Finally, curve 3 in Fig. 10(a) is the dielectric constant profile reconstructed from the reflectivity curve 1 in Fig. 10(b) with the use of our approach assuming only two points of discontinuity. A small variation in the profile as compared with the profile 2 appears to fit adequately the reflectivity curve over $\theta \sim 0.2^\circ - 0.45^\circ$. In other words, profiles 1 and 3 in Fig. 10(a) result in the same reflectivity curves over the whole range of the grazing angles, while the number of discontinuity points is different.

Notice however, that a change in the dielectric constant of the uppermost and lowermost films by only $+5\%$ and

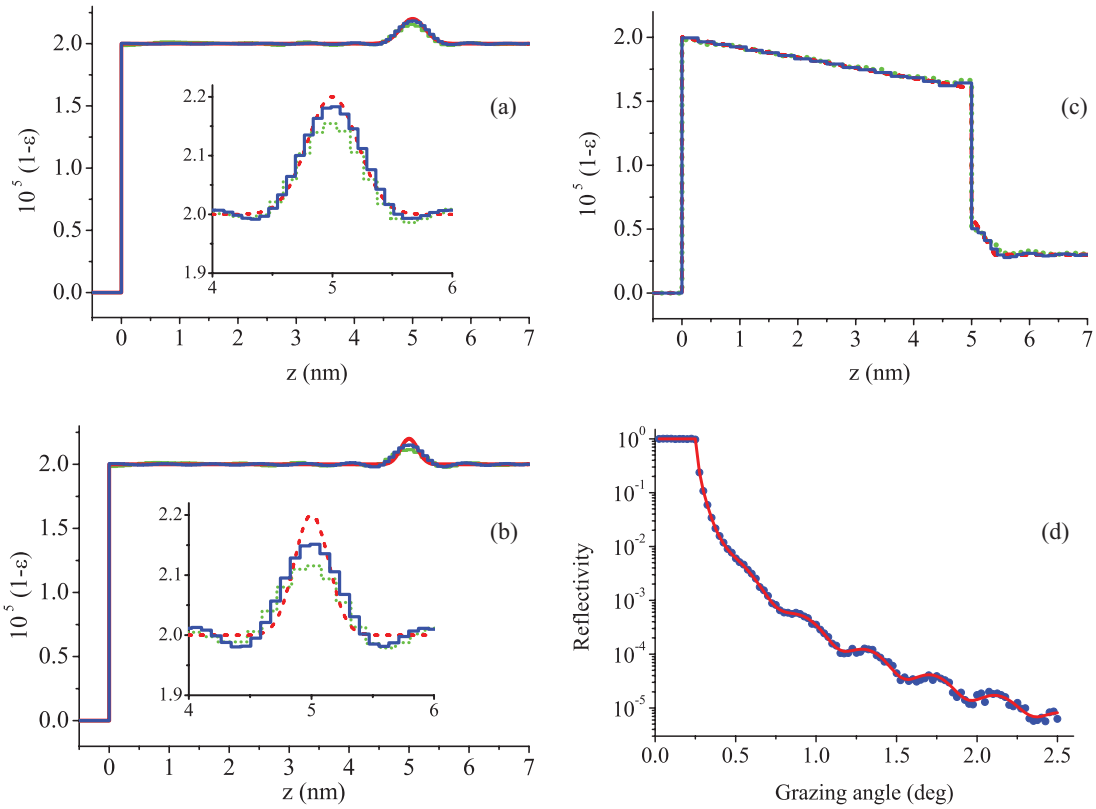

FIG. 11. (Color online) (a)–(c) Models of depth distribution of the dielectric function (dashed red curves). The reconstructed profiles are shown for $\theta_{max} = 2.5^\circ$ and $E = 17.5$ keV, i.e., $\lambda_{eff} \approx 1.6$ nm. The solid blue curve is obtained in absence of experimental error, while the dotted green one considers an error on the reflectivity measurements that increases from $\pm 2\%$ at small grazing angles up to $\pm 30\%$ at large grazing angles. The inserts (enlarged scale) demonstrate the accuracy of the reconstruction. (d) Reflectivity of a sample, whose dielectric constant depth profile is shown in Fig. 11(a), without (solid curve) and with (circles) an error introduced in the reflectivity data.

-5%, respectively, will result immediately in the appearance of two additional stable peaks at $x = 4$ nm and $x = 8$ nm [Fig. 10(d)], i.e., the situation becomes similar to reflectivity of a two-layer sample and can be analyzed as above. Therefore, an adequate model for the sample may be verified by performing anomalous reflectivity measurements, i.e., by measuring the reflectivity curves at two different x-rays energies lying below and above the absorption edge of one of the elements contained in the structure, where its polarizability changes essentially. It is unlikely that Eq. (A3) will be valid at both energies, and hence, we will observe three peaks of the function F(x) at one of these energies, at least.

APPENDIX B

One of the key issues in the reconstruction of the dielectric function profile concerns the depth resolution, i.e., the smallest feature size of the $\varepsilon(z)$-distribution that can be reconstructed from reflectivity measurements performed over a limited interval of grazing angles. The depth resolution $\Delta z_{min} = C\lambda_{eff}$ where $\lambda_{eff} = \lambda / \sin\theta_{max}$ is determined by the minimal effective wavelength characterizing the periodicity along the z axis of a wave field incident onto a sample under the maximal grazing angle θ_{max} obtainable in an experiment. The coefficient C proves to be often significantly lower than unity, expressing that the reconstructed feature size may be several times smaller than the effective radiation wavelength λ_{eff}. This statement is not surprising if we recall that a reflectivity curve measured as a function of the incidence angle is a recording of the interference pattern generated by the x-ray wave reflected from the different features of the dielectric constant profile. Interference techniques are known to reach spatial resolutions beyond the radiation wavelength used.

To illustrate this effect, let us consider an x-ray wave reflected from a substance of constant density except in a small region with a size of about 0.8 nm and placed at a certain depth in the sample [see Fig. 11(a), dashed red (dark gray) curve]. Let us consider angular reflectivity measurements performed up to a maximal value $\theta_{max} = 2.5^\circ$ at an x-ray energy of 17.5 keV. Then, the effective wavelength equals to $\lambda_{eff} \approx 1.6$ nm. The reflectivity corresponding to this model [Fig. 11(d), solid curve] demonstrates the presence of noticeable oscillations caused by the interference of waves reflected from the feature and from the top of the sample. As a result, the feature seen in the $\varepsilon(z)$-distribution is reconstructed with a high accuracy [Fig. 11(a), solid blue curve], although its size is two times less than the effective wavelength. As demonstrated with the red (dark gray) and blue curves in Fig. 11(b), where the feature size in the dielectric constant profile is about 0.55 nm, the accuracy of reconstruction is still reasonable for a feature with a size of the order of $\lambda_{eff}/3$. Figure 11(c), red (dark gray) curve, presents a model of $\varepsilon(z)$-distribution similar to

the dielectric constant profile obtained in our experiment with a thickness of the diffusion layer of only 0.4 nm, i.e., equal to $\lambda_{\text{eff}}/4$. Nevertheless, this layer is reconstructed quite precisely [Fig. 11(c), solid blue curve]. Therefore, the minimal size $\Delta z_{\min}$ of a reconstructed feature located in the depth of a sample is of the order of $(0.25 \div 0.35)\lambda_{\text{eff}}$. Let us recall once more that no additional assumptions about the $\varepsilon(z)$-distribution were made for reconstructing the dielectric function, except on the number of points of zero-order discontinuity (one or two) and on the distance between them [in the case of the profile shown in Fig. 11(c)]. The coefficient C characterizing the depth resolution depends on a number of factors, e.g., on the absolute depth position of a feature within a sample and on its shape. From an accuracy point of view, the worse situation corresponds to a feature placed at the top of the sample (then $C \approx 0.5$) and can even aggravate if the derivative $|d\varepsilon/dz|$ is large at $z = 0$ (then $C \approx 1$). Hence, the minimal size of a reconstructed feature placed on the top of a sample is $\Delta z_{\min} = (0.5 \div 1.0)\lambda_{\text{eff}}$.

Evidently, another factor influencing the accuracy of reconstruction of the dielectric function is the error present in the reflectivity measurements. Examples are given in Figs. 11(a)–11(c). The dotted green (gray) curves show the $\varepsilon(z)$-distributions reconstructed assuming a stochastic error on the reflectivity that is evenly distributed in an interval increasing from $\pm 2\%$ at small grazing angle up to $\pm 30\%$ at large angle. Although the exactitude of the reconstruction decreased, it is still practicable. An example of reflectivity curve (the sample corresponding to the dielectric constant depth profile shown in Fig. 11(a) in which an error was introduced is presented in Fig. 11(d) (circles).

A crucial factor decreasing the accuracy on the dielectric function reconstruction is the effect of the surface and interfacial roughness leading to a deformation of the reflectivity curve. As demonstrated in Ref. 9, the presence of roughness results in a smoothing of the reconstructed dielectric constant profile so that it becomes impossible to distinguish a real structure at an interface from an effect caused by roughness (if the study is only based on reflectivity measurements). This justifies the need to account for roughness during the reconstruction of the dielectric constant profile, as it is described in the present paper. In the conditions of our experiments, the minimum feature size correctly reconstructed is of the order of 0.4 to 0.5 nm for a feature located in the depth of the sample (diffusion layer near the top of the substrate).

---

*Present address: Société Européenne de Systèmes Optiques, Pôle d'Activité d'Aix les Milles, 13593, Aix en Provence Cedex 3, France.
†ziegler@esrf.fr

[1] U. Pietsch, V. Holy, and T. Baumbach, *High Resolution X-Ray Scattering: From Thin Films to Lateral Nanostructures* (Springer Verlag, New York, 2004).
[2] M. Tolan, in *X-Ray Scattering from Soft-Matter Thin Films. Materials Science and Basic Research*, edited by G. Höhler, (Springer, Berlin, 1999), Vol. 148, Chap. 3, pp. 33–73 and Chap. 6, pp. 114–49.
[3] L. Peverini, E. Ziegler, T. Bigault, and I. Kozhevnikov, Phys. Rev. B **72**, 045445 (2005).
[4] L. Peverini, E. Ziegler, T. Bigault, and I. Kozhevnikov, Phys. Rev. B **76**, 045411 (2007).
[5] L. Peverini, E. Ziegler, and I. Kozhevnikov, Phys. Status Solidi A **204**, 2785 (2007).
[6] D. S. Sivia, W. A. Hamilton, and G. S. Smith, Physica B **173**, 121 (1991).
[7] J. S. Pedersen and I. W. Hamley, J. Appl. Cryst. **27**, 36 (1994).
[8] E. Bengu, M. Salud, and L. D. Marks, Phys. Rev. B **63**, 195414 (2001).
[9] I. V. Kozhevnikov, Nucl. Instrum. Methods A **508**, 519 (2003).
[10] I. V. Kozhevnikov, L. Peverini, and E. Ziegler, J. Appl. Phys. **5**, 054914 (2008); Opt. Express **16**, 144 (2008).
[11] The notion of PSD function is familiar to various fields, including the theory of stochastic processes [M. C. Teich, S. B. Lowen, B. M. Jost, K. Vibe-Rheymer, and C. Heneghan, in *Nonlinear Biomedical Signal Processing: Dynamic Analysis and Modeling*, edited by M. Akay (IEEE Press, New York, 2001), Vol. 2, Chap. 6, pp. 159–213; the theory of radiation scattering by roughness P. Beckmann and A. Spizzichino, *The Scattering of Electromagnetic Waves from Rough Surfaces* (The Macmillan Co., New York, 1963), pp. 107; J. M. Bennett and L. Mattson, *Introduction to Surface Roughness and Scattering* (Optical Society of America, Washington DC, 1989), pp. 48–53; and in the analysis of the statistical properties of rough surfaces from atomic force microscopy measurements C. Ruppe and A. Duparre, Thin Solid Films **288**, 8 (1996)].
[12] S. K. Sinha, E. B. Sirota, S. Garoff, and H. B. Stanley, Phys. Rev. B **38**, 2297 (1988).
[13] I. V. Kozhevnikov and M. V. Pyatakhin, J. X-Ray Sci. Technol. **8**, 253 (2000).
[14] V. E. Asadchikov, I. V. Kozhevnikov, Yu. S. Krivonosov, R. Mercier, T. H. Metzger, C. Morawe, and E. Ziegler, Nucl. Instrum. Methods A **530**, 575 (2004).
[15] A. N. Tikhonov and V. Ya. Arsenin, *Approaches to Solving of Ill-Conditioned Problems* (Nauka, Moscow, 1979) [in Russian].
[16] E. L. Church and P. Z. Takacs, in *Handbook of Optics*, edited by M. Bass (McGraw-Hill, New York, 1995), Vol. 1, pp. 7.1–7.14.